PERGAMON

International Journal of Multiphase Flow 27 (2001) 1707–1734

International Journal of Multiphase Flow

www.elsevier.com/locate/ijmulflow

Nonlinear capillary waves on swirling, axisymmetric free liquid films

Carsten Mehring, William A. Sirignano *

Department of Mechanical and Aerospace Engineering, University of California at Irvine, Irvine, CA 92697, USA

Abstract

The nonlinear distortion and breakup of a swirling axisymmetric thin inviscid liquid sheet in a void and at zero gravity is analyzed by means of a reduced dimension approach. Nonlinear steady-state solutions are presented for various boundary conditions imposed at the nozzle exit. Unsteady solutions describing the nonlinear breakup of the radially expanding film due to dilational or sinuous modulations at the nozzle exit are presented. Fluid rings with thin connecting shells are formed due to nonlinear effects and sheet thinning caused by sheet divergence is found to increase nonlinear breakup lengths and times for both sinuous and dilational modes. For the case of a swirling annular liquid sheet, comparisons are made with an annular sheet which is stabilized by a constant gas-core pressure. Here, swirl causes a reduction in breakup lengths and times.

Keywords: Liquid film stability; Capillary waves; Liquid atomization; Swirl injection

1. Introduction and problem formulation

The stability of liquid sheets plays an important role in various technological applications including spray combustion of liquid fuels in furnaces, internal combustion piston engines, jet engine combustion chambers and rocket motors (Lefebvre, 1989). The combustion of liquid fuels in the prescribed applications is frequently achieved through the generation and disintegration of swirling conical liquid films (Fraser, 1956).

Experimental observations of disintegrating conical liquid sheets have already been described by York et al. (1953) and Squire (1953) in context with comparisons to their linear temporal

* Corresponding author. Tel.: +1-949-824-3700; fax: +1-949-824-3773.
E-mail address: sirignan@uci.edu (W.A. Sirignano).

0301-9322/01/$ - see front matter
PII: S0301-9322(01)00034-9

stability analyses of planar sheets in an ambient gas stream. [1] Both authors report qualitative and/or satisfactory quantitative agreement between experimental observations and their theoretical predictions of film break-up by aerodynamic effects (i.e. wave formation and growth). In particular, York et al. (1953) note that, in agreement with their analysis, an increase in sheet velocity leads to more regular wave forms and shorter breakup lengths. Squire (1953) clarifies that his linear theory for antisymmetrical waves does not give an indication of how rupture of the film takes place. [2] A phenomenological description of the breakup process of conical sheets was given by York et al. (1953). The authors illustrate that aerodynamic wave growth causes rings and holes to appear on the sheet, resulting in the formation of liquid rings which subsequently disintegrate solely under the action of capillary forces (Rayleigh breakup). As noted, the prescribed cylindrical instability begins to operate before aerodynamic wave growth tears the sheet apart. York et al. (1953) and Squire (1953) stress that their linear analyses break down when unstable waves have grown to an appreciable size.

Squire (1953) also indicates that sheet breakup for low ambient pressure and/or fuel pressure does not appear to be related to the instability of wave-motion (i.e. aerodynamic effects). In this context, the role of capillary waves found near the nozzle exit was later discussed by Taylor (1959b). Capillary waves on conical sheets and close to the nozzle exit were also observed by York et al. (1953) and have been studied later by Hashimoto and Suzuki (1991) for the case of discharging planar sheets. In context with aerodynamic wave growth, York et al. (1953) show that the growth of short-wavelength disturbances required for the generation of small drops can only be achieved by high relative velocities between the liquid film and the surrounding gas, providing some explanation to the question why spray producing apparatus generally convert only a small amount of the energy supplied into surface energy.

In his third paper in a series of three, Taylor (1959b) considers the dynamics of free edges on liquid sheets with uniform or spatially varying thickness. For conical sheets produced by a swirl atomizer, Taylor (1959b) reports that its thickness fluctuates greatly where it emerges from the orifice. The edge of the conical sheet establishes itself, as illustrated, at a radius (i.e. radial distance from the symmetry axis) well below the value predicted by his 'edge-dynamics' theory. The edge location is given by the location where surface tension forces and inertia forces acting on a fluid element (at the free edge) are balanced, i.e. where $(2\sigma/\rho\bar{t})^{1/2} = u$ or $We = \rho\bar{t}u^2/(2\sigma) = 1$. Here, u denotes the sheet velocity and $\bar{t}$ represents the mean sheet thickness. Note that on a sheet of uniform thickness, the left-hand-side of the previous equation corresponds to the velocity of antisymmetrical waves propagating on the sheet. For the continuous part of the conical sheet, Taylor (1959b) reports good agreement between the experimentally observed shape and predictions obtained for a water bell with the same 'discharge' angle (Taylor, 1959a). However, experimental predictions for the Weber number We at the breakup point are found to be significantly larger than the theoretically predicted value $We = 1$. Taylor explains this discrepancy with the

[1] Note that Squire (1953) analyzes the sinuous mode of sheet distortion, whereas York et al. (1953) consider the deformation of only one side of the free liquid sheet, whereby the other side is assumed to remain undisturbed.

[2] As reported, the author also studied the symmetric mode of sheet distortion. However, the growth rates for this mode were found to be significantly smaller than those for the analyzed antisymmetric mode.

existence of variations in the sheet thickness (dilational waves) which effectively increase the resultant mean velocity of the edge.

Taylor offers two explanations for the origin of the observed thickness variations: (1) a lack of symmetry in the steady flow in the orifice and (2) oscillations of the air core which is formed within the orifice. The latter, so Taylor (1959b) states, might explain the appearance of streaks at nearly right angles to the axis of the experimentally observed liquid cone. As noted, the variations in thickness will determine the mean value of *We* at the point where breakup occurs. Note that, Taylor (1959b) only considers capillary and inertia forces. Gas phase effects were only considered in context with the prediction of the liquid-bell shape (Taylor, 1959a), where the effect of air drag was included in the analysis.

In the past, theoretical analyses of the phenomenon of liquid-film breakup were in general limited to linear planar or annular sheet configurations; the latter with or without swirl (Panchagnula et al., 1996). The few nonlinear analyses presented on the subject were also limited to the planar geometry (Mehring and Sirignano, 1999; Kim and Sirignano, 2000), annular sheets, or liquid bells without swirl (Lee and Wang, 1986, 1989; Ramos, 1992; Mehring and Sirignano, 2000a,b; Panchagnula et al., 1998). Analyses presented by Ramos (1992, 1994, 1995a,b,c,d, 1996a,b,c,d, 1997a,b, 1998, 1999) and Panchagnula et al. (1995, 1996, 1998) did not consider wave phenomena (linear or nonlinear) on diverging (i.e., continuously thinning) axisymmetric sheets. With the exception of one analysis (Ramos, 1997a), none considered modulations imposed onto the sheets at the nozzle exit. However, both divergence and modulation are very important to the atomization process (e.g., in pressure-swirl atomizers) and are considered within our work. In his analysis on the effect of liquid flow rate fluctuations on the mass transfer between an annular collapsing liquid sheet and its gas core, Ramos (1997a) considered modulations of the axial velocity component at the nozzle. However, the author was not interested in the liquid break-up phenomenon, and although the governing equations were nonlinear, nonlinear effects with respect to the interface distortion were small. In his analyses, Ramos was primarily interested in heat and mass transfer between collapsing annular liquid sheets and their reacting gas core, the effect of fluctuating body forces on this flow configuration and the existence of singularities within the steady-state liquid phase equations. Previous analyses by Panchagnula and co-workers were linear with the exception of the work by Panchagnula et al. (1998), the latter being confined to dilationally distoring nonswirling, nondiverging annular sheets subject to time-independent boundary conditions at the nozzle exit. A theoretical analysis of the nonlinear breakup process for conical liquid sheets has not been presented so far. The present work provides such an analysis.

In the analysis of thin liquid sheets or films presented here, only capillary and inertia effects are considered. Subsequently, the term 'annular' refers to thin-walled cylindrical liquid columns with ring-shaped cross-sectional area of constant time-averaged radius along the axial direction. Sheets or films which resemble hollow cones (although not necessarily geometrically exactly), i.e., thin walled liquid columns with monotonically increasing or decreasing annular radius of the ring-shaped cross-sectional area, are named 'conical' sheets. Clearly, sheets or films discharging from an annular nozzle and with a monotonically increasing or decreasing annular radius within the area of interest next to the atomizer are still referred to as being 'conical' even if the annular radius undergoes oscillations further downstream. The latter phenomenon might occur due to the dynamic exchange of translational or rotational kinetic energy and potential or surface energy.

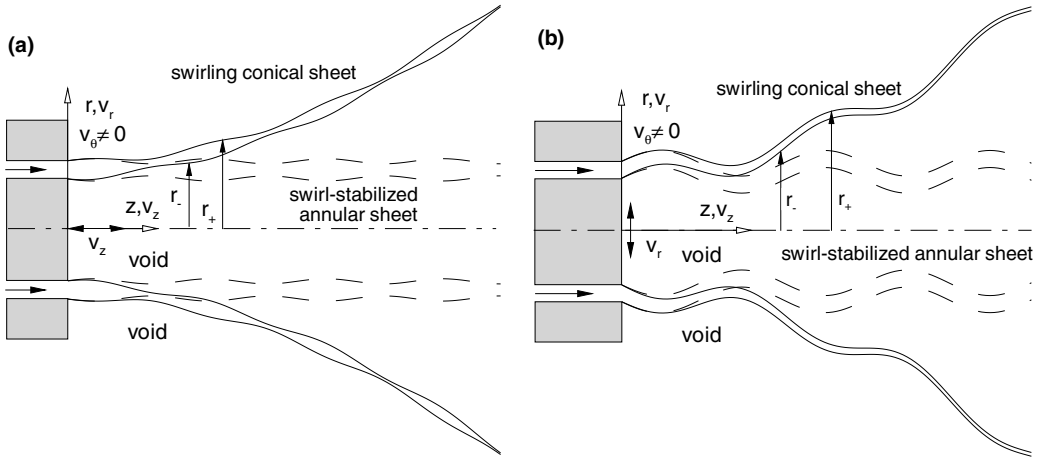

Fig. 1. Schematic depictions of the investigated semi-infinite annular and conical sheet configurations: (a) dilational modulation and (b) sinuous modulation.

The work presented here is an extension of previous work by the authors on thin planar and annular liquid sheets (Mehring and Sirignano, 1999, 2000a,b). Considered is a semi-infinitely long thin swirling liquid film, exiting from an annular nozzle or atomizer as shown in Fig. 1. Axisymmetric dilational and sinuous disturbances are considered. Liquid viscosity is neglected and the sheet is exiting into a void under negligible gravity. The assumption of thin sheets allows the reduction of the dimensionality of the problem by integrating across the thickness of the sheet. The same approach has been employed by Ramos (1992) and by the authors for the analyses of thin planar and annular sheets without swirl (Mehring and Sirignano, 1999, 2000a,b). Only spatial stability will be of interest here. The spatially periodic temporal instability is not relevant to the conical sheet with its varying radius. The temporal instability can apply to the annular cylindrical sheet and for the radially expanding sheet.

2. Governing equations

The governing equations, describing the unsteady motion in an incompressible, inviscid axisymmetric liquid sheet under zero gravity and in a cylindrical coordinate system, are given by

$$\frac{1}{r}\frac{\partial}{\partial r}(rv_r)+\frac{\partial v_z}{\partial z}=0, \tag{1}$$

$$\frac{\partial v_z}{\partial t}+\frac{\partial v_z^2}{\partial z}+\frac{1}{r}\frac{\partial}{\partial r}(rv_zv_r)=-\frac{1}{\rho_1}\frac{\partial p}{\partial z}, \tag{2}$$

$$\frac{\partial v_r}{\partial t}+\frac{1}{r}\frac{\partial}{\partial r}(v_r^2r)+\frac{\partial}{\partial z}(v_zv_r)-\frac{v_\theta^2}{r}=-\frac{1}{\rho_1}\frac{\partial p}{\partial r}, \tag{3}$$

$$\frac{\partial v_\theta}{\partial t}+v_r\frac{\partial v_\theta}{\partial r}+v_z\frac{\partial v_\theta}{\partial z}+\frac{v_rv_\theta}{r}=0, \tag{4}$$

where v_z, v_r and v_θ are the velocity components in the axial (z-), radial (r-) and circumferential (θ-) directions, respectively (see Fig. 1). p and ρ_l denote the pressure and the density of the liquid.

Indicating the outer and inner location of the sheet by $r_+(z,t)$ and $r_-(z,t)$, we define the radial centerline position and the thickness of the sheet by $\bar{r}(z,t) = (r_+ + r_-)/2$ and $\Delta r(z,t) = r_+ - r_-$. The pressure and the radial velocity component at the fluid interfaces ($p_\pm, v_{r,\pm}$) are given by the following kinematic and dynamic boundary conditions:

$$v_{r,\pm} = \frac{\partial r_\pm}{\partial t} + v_{z,\pm}\frac{\partial r_\pm}{\partial z}, \tag{5}$$

$$p_\pm = p_{g,\pm} \pm \sigma\left(\frac{1}{R_{1,\pm}} + \frac{1}{R_{2,\pm}}\right) = p_{g,\pm} \mp \sigma\frac{\partial^2 r_\pm}{\partial z^2}\left[1 + \left(\frac{\partial r_\pm}{\partial z}\right)^2\right]^{-3/2} \pm \frac{\sigma}{r_\pm}\left[1 + \left(\frac{\partial r_\pm}{\partial z}\right)^2\right]^{-1/2}, \tag{6}$$

where R_1 and R_2 denote the first and second radius of curvature, p_g is the pressure of the surrounding gas ($p_{g,\pm} = 0$ here) and σ denotes the surface tension coefficient of the liquid. The subscripts "+" and "−" denote values at the outer and inner interface of the liquid sheet. Note that within the analysis by Mehring and Sirignano (2000a,b), $p_{g,-} - p_{g,+} > 0$ in order to stabilize the nonswirling annular sheet in its undisturbed configuration ('pressure stabilization'). This is in contrast to the present analysis of 'swirl-stabilized' annular sheets in a void. Here, the undisturbed annular sheet configuration is stabilized by centrifugal forces due to swirl.

We can assume an analytical behavior of the governing equations away from $r = 0$, as a function of r. Also, assuming that the sheet thickness is small compared to the streamwise disturbance wavelength, it is consistent to consider v_z and v_θ to be nearly constant and v_r and p to be linearly varying with r. It is convenient, therefore, to reduce the problem to a one-dimensional, unsteady formulation by integrating Eqs. (1)–(4) over the sheet thickness. This is done by using Leibnitz's rule and by considering the previously mentioned velocity and pressure profile approximations. Introducing averaged quantities $\overline{\phi}$, defined by

$$\overline{\phi} \equiv \frac{\int_{r_-}^{r_+}(\phi 2\pi r)\,\mathrm{d}r}{\int_{r_-}^{r_+} 2\pi r\,\mathrm{d}r} = \frac{\int_{r_-}^{r_+}(\phi r)\,\mathrm{d}r}{\bar{r}\Delta r} \tag{7}$$

one obtains

$$\frac{\partial \Delta r}{\partial t} + \frac{\partial(\overline{v}_z \Delta r)}{\partial z} = -\frac{\Delta r}{\bar{r}}\overline{v_r}, \tag{8}$$

$$\frac{\partial \overline{v}_z}{\partial t} + \overline{v}_z\frac{\partial \overline{v_z}}{\partial z} = -\frac{1}{\rho_l}\left[\frac{\partial \overline{p}}{\partial z} - \Delta p\left(\frac{1}{\Delta r}\frac{\partial \bar{r}}{\partial z} + \frac{1}{4\bar{r}}\frac{\partial \Delta r}{\partial z}\right)\right], \tag{9}$$

$$\frac{\partial \overline{v}_r}{\partial t} + \overline{v}_z\frac{\partial \overline{v}_r}{\partial z} = -\frac{1}{\rho_l}\frac{\Delta p}{\Delta r} + \frac{\overline{v}_\theta^2}{\bar{r}}, \tag{10}$$

$$\frac{\partial \overline{v}_\theta}{\partial t} + \overline{v}_z\frac{\partial \overline{v}_\theta}{\partial z} = -\frac{\overline{v}_r\overline{v}_\theta}{\bar{r}}, \tag{11}$$

$$\frac{\partial \bar{r}}{\partial t} + \overline{v}_z\frac{\partial \bar{r}}{\partial z} = \overline{v}_r \tag{12}$$

with $\Delta p = p_+ - p_-$ and $\overline{p} = (p_+ + p_-)/2$ given by

$$\overline{p} = -\frac{\sigma}{2}\left[\frac{G_+ + G_-}{2}\frac{\partial^2 \Delta r}{\partial z^2} + (G_+ - G_-)\frac{\partial^2 \overline{r}}{\partial z^2} + \frac{1}{D}\left[\frac{F_+ + F_-}{2}\Delta r - (F_+ - F_-)\overline{r}\right]\right], \tag{13}$$

$$\Delta p = -\sigma\left[(G_+ + G_-)\frac{\partial^2 \overline{r}}{\partial z^2} + \frac{G_+ - G_-}{2}\frac{\partial^2 \Delta r}{\partial z^2} - \frac{1}{D}\left[(F_+ + F_-)\overline{r} - \frac{F_+ - F_-}{2}\Delta r\right]\right], \tag{14}$$

where $D = \overline{r}^2 - \Delta r^2/4$ and $F_\pm$ and $G_\pm$ are given by

$$F_\pm = G_\pm^{1/3}, \tag{15}$$

$$G_\pm = \left[1 + \left(\frac{\partial \overline{r}}{\partial z}\right)^2 \pm \frac{\partial \overline{r}}{\partial z}\frac{\partial \Delta r}{\partial z} + \frac{1}{4}\left(\frac{\partial \Delta r}{\partial z}\right)^2\right]^{-3/2}. \tag{16}$$

Eqs. (8)–(16) form a closed system of equations which together with appropriate boundary and initial conditions govern the nonlinear distortion of thin axisymmetric liquid sheets exiting from a nozzle or atomizer into a void. Sheet break-up occurs when the independent variable for the sheet thickness reaches zero value locally. For the subsequent analyses, the above equations have been nondimensionalized by using the sheet thickness and axial velocity component at the nozzle exit, i.e. Δr_0 and $\overline{v_z}_{,0}$, as characteristic length and velocity. The Weber number in the resulting non-dimensional equations is then given by $We = \rho_l \overline{v_z}_{,0}^2 \Delta r_0/\sigma$.

It has previously been shown by the authors (Mehring and Sirignano, 1999) that, for the case of a planar sheet, the employed assumptions for the velocity and pressure profiles across the sheet agree with the lowest-order expansion of the full two-dimensional problem in terms of $(y - \overline{y})/\lambda$, where y denotes the direction perpendicular to the undisturbed sheet, $\overline{y}(x,t)$ is the instantaneous location of the sheet centerline in the y-direction and λ is the wavelength of a disturbance in the x-direction. In other words, for the planar case the reduced-dimension equations are exact in the limit where the ratio between sheet thickness and λ reaches zero.

For steady-state annular liquid membranes with sinuous distortions, the analogy between integral (control-volume) formulation and rigorous Taylor series expansions has been demonstrated by Ramos (1996d). The integral representation employed by the authors for nonswirling annular sheets (Mehring and Sirignano, 2000a,b) follows, as mentioned earlier, Ramos' analysis for the steady version of the configuration (Ramos, 1992) but extends it to the unsteady cases of both sinuous and dilational sheet distortions.

The limitations of the employed formulation, in particular during pinch-off (when short wavelength disturbances cannot be neglected) have been addressed in this previous work (Mehring and Sirignano, 2000a,b). It is noted however that, despite these constraints, the usefulness of the approach has been demonstrated conclusively for planar sheets, by comparison with accurate two-dimensional vortex-dynamics simulations (Mehring and Sirignano, 1999).

3. Results and discussion

3.1. Annular sheets / modal analysis

Considering swirl-stabilized annular sheets only, [3] linearization of Eqs. (8)–(16) yields

$$\frac{\partial h}{\partial t^*}+\frac{\partial h}{\partial z^*}+\frac{\partial u}{\partial z^*}=-\frac{1}{R}v, \tag{17}$$

$$\frac{\partial u}{\partial t^*}+\frac{\partial u}{\partial z^*}=\varepsilon^2\left\{\frac{\partial^3 h}{\partial z^{*3}}+\frac{1}{R^2}\frac{\partial h}{\partial z^*}+\frac{4}{R}\frac{\partial r}{\partial z^*}\right\}, \tag{18}$$

$$\frac{\partial v}{\partial t^*}+\frac{\partial v}{\partial z^*}-\frac{2}{R}w_0 w+\frac{w_0^2}{R^2}r=\varepsilon^2\left\{4\frac{\partial^2 r}{\partial z^{*2}}+4\frac{r}{R^2}+\frac{4}{R}h\right\}, \tag{19}$$

$$\frac{\partial r}{\partial t^*}+\frac{\partial r}{\partial z^*}=v, \tag{20}$$

$$\frac{\partial w}{\partial t^*}+\frac{\partial w}{\partial z^*}=-\frac{w_0}{R}v \tag{21}$$

if terms of $O(R^{-3})$ are neglected. Here, h, r, u, v and w denote fluctuations of the dependent variables written in nondimensional form, [4] i.e. $\Delta r^*=1+h$, $\overline{r}^*=R+r$, $\overline{u}^*=1+u$, $\overline{v}^*=v_0+v$, and $\overline{w}^*=w_0+w$, where $v_0=0$ and $w_0=2\varepsilon R(R^2-0.25)^{-0.5}$ is the azimuthal velocity necessary to stabilize the undisturbed annular sheet with radius R. ε is representative for the square root of the inverse Weber number and is given by $\varepsilon=1/\sqrt{2We}$. Note that, the characteristic length and velocity used within the nondimensionalization process are the thickness of the annular sheet at the nozzle exit and its undisturbed axial velocity. Accordingly, R and w_0 denote ratios between annular radius and sheet thickness or circumferential and axial velocity, respectively. Eqs. (17) and (18) govern the dilational mode and differ from the equations derived previously for pressure-stabilized annular sheets (Mehring and Sirignano, 2000b) by the additional term $4/R\,\partial r/\partial z^*$ within Eq. (18). This term couples the dilational with the sinuous mode of sheet distortion, latter being described by Eqs. (19)–(21). In Eq. (19), coupling with the dilational mode occurs through the term $(4\varepsilon^2/R)h$. This is in contrast to pressure-stabilized annular sheets (Mehring and Sirignano, 2000a,b) where mode coupling only occurred through the right-hand side of the conservation-of-mass Eq. (17) if terms of $O(R^{-3})$ and higher are neglected. Differences in the linearized equations between pressure-stabilized annular sheets (i.e., sheets which are stabilized by a constant pressure difference between gas-core and surrounding gas) and swirl-stabilized sheets appear through additional terms within the governing equation for u and v, and the existence of an additional equation for the azimuthal velocity fluctuation w if swirl is present.

According to the coupling between dilational and sinuous modes, and in contrast to pressure-stabilized nonswirling annular sheets, dispersion relations for the dilational and sinuous modes cannot be obtained separately for swirl-stabilized annular sheets. Assuming solutions of the form

[3] A modal analysis of the 'conical' case, i.e. annular sheets in a void and with more swirl at the nozzle exit than needed to stabilize the annular configuration, is not readily available since the corresponding linearized solution for the base-flow does not separate into classical functions.

[4] Superscript '*' denotes a nondimensional quantity.

$h = h^0 e^{i(\omega t^* - k z^*)}$, $u = u^0 e^{i(\omega t^* - k z^*)}$, $r = r^0 e^{i(\omega t^* - k z^*)}$, $v = v^0 e^{i(\omega t^* - k z^*)}$, and $w = w^0 e^{i(\omega t^* - k z^*)}$ the overall dispersion relation for the considered swirl-stabilized annular liquid sheets is given by

$$(w-k)\left\{\left[(w-k)^2 - 4\varepsilon^2\left(\frac{2}{R^2}+k^2\right)\right]\left[(w-k)^2 + \varepsilon^2 k^2\left(\frac{1}{R^2}-k^2\right)\right] - \frac{4}{R^2}\varepsilon^2\left[(w-k)^2 + 4\varepsilon^2 k^2\right]\right\} = 0, \tag{22}$$

where $w_0 = 2\varepsilon R(R^2 - 0.25)^{-1/2} \approx 2\varepsilon$ (since terms of order R^{-3} have been neglected). For spatially developing annular sheets exiting from a nozzle or atomizer (considered here), the above dispersion relation has to be solved for wavenumber k as a function of ω, the latter being the frequency at which harmonic time-dependent fluctuations are imposed at the nozzle exit. Eq. (22) provides seven solutions for wavenumber k, whereby the $k = \omega$ solution branch represents an uninteresting sinuous disturbance which does not move relative to the fluid and which is generated by fluctuations of the swirl- or azimuthal-velocity w at the nozzle exit. For the parameter range considered in this paper, the remaining wavenumber solutions k describe four predominantly dilational and two predominantly sinuous waves. The wavenumbers for the 'sinuous mode' are subsequently referred to as l_1 and l_2. Here, a wavenumber is said to produce a predominantly dilational or sinuous wave if the ratio of the amplitudes in h and r, i.e. h^0/r^0, pertaining to the particular wavenumber is significantly larger or smaller than one.

The wavenumbers which produce predominantly dilational waves behave qualitatively the same as the corresponding purely dilational waves on pressure-stabilized annular sheets, the latter being governed by Eq. (6) of Mehring and Sirignano (2000b). However, the range of unstable "dilational" wavenumbers for swirl-stabilized sheets is significantly larger than for the pressure-stabilized case. For pressure-stabilized sheets with $R = 10$ and $We = 5$, instability is found if $\omega < 0.1$; for the similar swirl-stabilized case the instability range extends to $\omega < 0.425$. The maximum growth rate for the swirl-stabilized sheet is about sixty times larger than the maximum growth rate predicted for the pressure-stabilized sheet in this case. Qualitative differences between the solutions to Eq. (22) and the solutions to the dispersion relation for dilational waves on pressure-stabilized sheets (Eq. (6), Mehring and Sirignano, 2000b) are found for large values of ω (e.g. $\omega > 0.6$ for $R = 10, We = 5$). However, short-wavelength disturbances resulting from the imposed sheet modulation render the validity of the employed long-wavelength approximation questionable in this case. For smaller Weber numbers qualitative differences can be observed even at smaller forcing frequencies ω (e.g. $\omega < 0.1$ for $We = 2.1$). However, as described below, low Weber number cases are not subject of the present investigation.

According to Eq. (22) and within the parameter range considered here, exponential behavior for predominantly sinuous mode disturbances is only possible for large ε-values; the bifurcation value is approximately $\varepsilon = 0.5$ ($We = 2$), but depends on R. This is in strong contrast to pressure-stabilized annular sheets, where unstable sinuous waves can only be found for $\varepsilon < 0.5$ (Mehring and Sirignano, 2000b). Figs. 2 and 3 illustrate the dependency of wavenumbers l_i on forcing frequency ω for predominantly sinuous waves on swirl- and pressure-stabilized annular sheets for two values of ε: $\varepsilon = 1/\sqrt{2}$ and $\varepsilon = 1/\sqrt{10}$. Note that Eq. (22) recovers the dispersion relations for sinuous and dilational waves on planar sheets (Mehring and Sirignano, 1999) in the limit where R is infinite.

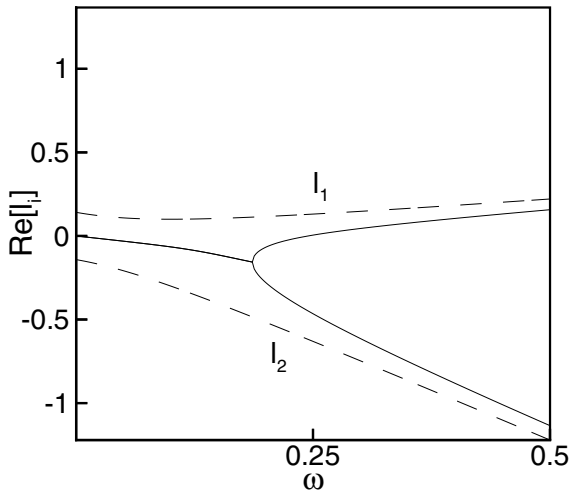

Fig. 2. Real values of 'sinuous mode' wavenumbers l_i, i.e. $\mathrm{Re}[l_i]$ with dependence on ω for $R = 10$ and $We = 1$: (solid): swirl-stabilized case, (dashed): annular pressure-stabilized case.

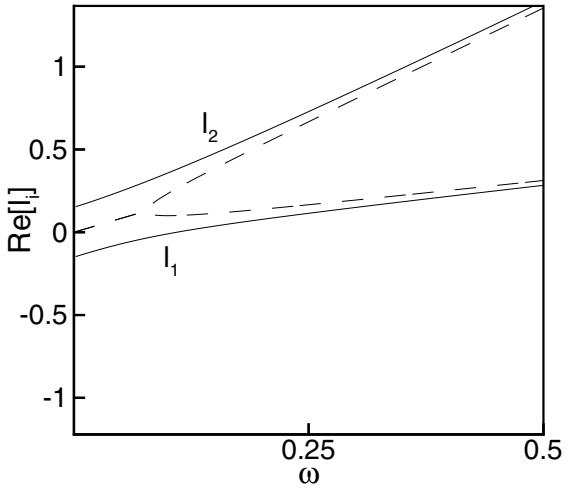

Fig. 3. Real values of 'sinuous mode' wavenumbers l_i, i.e. $\mathrm{Re}[l_i]$ with dependence on ω for $R = 10$ and $We = 5$: (solid): swirl-stabilized case, (dashed): annular pressure-stabilized case.

Analogous to the analyses of planar sheets (Mehring and Sirignano, 1999) and pressure-stabilized annular sheets (Mehring and Sirignano, 2000a,b), group velocity arguments can now be used to determine which wavenumbers are relevant for the solution downstream from the nozzle exit where a harmonic modulation at a given forcing frequency ω is imposed onto the swirl-stabilized annular sheet. For sinuous modulations and $\varepsilon = 1/\sqrt{10}$ (< 0.5), Fig. 3 illustrates that both wavenumber solutions are associated with positive group velocities $C(l_i) = \mathrm{d}\omega(l_i)/\mathrm{d}\,\mathrm{Re}[l_i]$, where $\mathrm{Re}[l_i]$ implies the real part of l_i. Accordingly, both wavenumbers will appear downstream

from the nozzle exit. For $\varepsilon = 1/\sqrt{2}$ (> 0.5) however, Fig. 2 shows that for complex conjugate values l_i (i.e. where $\mathrm{Re}[l_1]$ and $\mathrm{Re}[l_2]$ are represented by the same branch), $C(l_i) < 0$, implying that no one of these waves is part of the time-periodic solution to the considered boundary-value problem. Similarly, for real values of wavenumbers l_i and $\varepsilon = 1/\sqrt{2}$ (> 0.5), only wavenumber l_1 is expected to be part of the solution, since l_2 is associated with waves having negative group velocities. Note that, for the parameter range considered within the subsequent analyses,dilational waves on swirl-stabilized and pressure-stabilized annular sheets behave qualitatively the same, implying that the relevance of certain wavenumbers k_i to the linear problem at hand is the same as for the pressure-stabilized annular sheets described by Mehring and Sirignano (2000b).

Analogous to the analyses of spatially developing planar or pressure-stabilized annular sheets, wavenumbers l_i or k_i with $C(l_i, k_i) < 0$ are associated with energy transport upstream from infinity. According to Sommerfeld's radiation condition these wavenumbers have to be excluded from the solution to the considered boundary value problem.See, for example, Mehring and Sirignano (1999). Later, calculations will be presented for the annular sheet as a special case of the conical sheet.

The use of group-velocity arguments to exclude certain wavenumbers for the solution of the pure boundary-value problem might need reconsideration within the analysis of the corresponding initial- and boundary-value problem where group velocity information is used to determine the number of boundary conditions to be specified at the nozzle exit (Mehring and Sirignano, 2000b). This is particularly true for low Weber number cases where transient effects might cause the sheet to become absolutely unstable.

3.2. Radially expanding annular sheets

We now consider the uniform radial expansion of an annular sheet due to excess swirl. In other words, a cylindrical swirling liquid film is analyzed for which the amount of swirl initially present exceeds the amount needed to stabilize the film at its initial annular radius. The generation of a radially expanding cylindrical liquid layer, as considered here and generally referred to as film blowing, is one of the basic elements of polymer processing (Tadmor and Gogos, 1979). In this context, the prescribed process of film expansion due to excess swirl can be categorized as inertial (or impulse) expansion which is in contrast to the more frequent use of an increased gas pressure within the cavity formed by the annulus in order to generate the expansion.

For annular sheets with radial displacement only and without sheet disturbances in the axial direction, we have $\overline{v_z} = 0$ and $\partial(\ldots)/\partial z = 0$, so that Eqs. (8)–(12) can be rewritten as follows:

$$\frac{\mathrm{d}\Delta r}{\mathrm{d}t} = -\frac{\Delta r}{\overline{r}}\,\overline{v}_r,$$

$$\frac{\mathrm{d}\overline{v_r}}{\mathrm{d}t} = -\frac{2\sigma}{\rho_1}\,\frac{\overline{r}}{\Delta r\,(\overline{r}^2 - \Delta r^2/4)} + \frac{\overline{v_\theta}^2}{\overline{r}},$$

$$\frac{\mathrm{d}\overline{v_\theta}}{\mathrm{d}t} = -\frac{\overline{v_\theta}\,\overline{v_r}}{\overline{r}},$$

$$\frac{\mathrm{d}\overline{r}}{\mathrm{d}t} = \overline{v_r},$$

whereby an equation for $\overline{v}_z$ has no longer to be solved. The above system of equations can be simplified to yield

$$\Delta r\overline{r} = e_1, \tag{23}$$

$$\overline{v_\theta}\,\overline{r} = e_2, \tag{24}$$

$$\frac{\mathrm{d}^2\overline{r}}{\mathrm{d}t^2} = -\frac{2\sigma}{\rho_1}\frac{1}{e_1} + \frac{e_2^2}{\overline{r}^3}, \tag{25}$$

where the approximation $\overline{r}^2 - \Delta r^2/4 \approx \overline{r}^2$ has been made. The constant values e_1 and e_2 in Eqs. (23) and (24) are determined by the initial geometry of the cylindrical sheet and the angular momentum or swirl imposed at $t = 0$. Eq. (25) can be used to obtain the instantaneous annular radius of the film once its initial value $\overline{r}(t = 0)$ and its initial time-rate of change $\mathrm{d}\overline{r}/\mathrm{d}t(t = 0)$ have been specified. Eq. (25) shows that, depending on the initial swirl prescribed by e_2, the initial geometry prescribed by e_1, and the liquid properties (i.e., surface tension coefficient σ and density ρ_l), sheet collapse is possible, whereas continuous sheet blowout is not possible.

It can be shown that an oscillatory behavior for the temporal variation of $\overline{r}$ occurs around the equilibrium location $\overline{r}_s = We_s^{1/3}\overline{r}_0$ (assuming $\mathrm{d}\overline{r}/\mathrm{d}t = 0$ initially), whereby the swirl Weber number We_s is formed by $\overline{v_\theta}(t = 0)$, $\Delta r/2(t = 0)$, σ and ρ_l. If $We_s < 1$, radial acceleration of the sheet is initially inwards (towards $\overline{r}_s$); if $We_s > 1$, the sheet accelerates radially outwards towards its equilibrium position at $\overline{r}_s$. In the former case, sheet collapse, i.e. the formation of a "full" cylindrical jet, might occur, depending on the prescribed problem parameters as well as on $\overline{r}_0$ and $\mathrm{d}\overline{r}/\mathrm{d}t$ at $t = 0$. On the other hand, sheet instability leading to continuous radial sheet blowout is not possible for swirling annular sheets subject to inertia and capillary forces only. In contrast, a nonswirling annular sheet, stabilized at $\overline{r}_0$ by a constant pressure difference between inner gas core and the surrounding gas phase, is neutrally stable and any deviation from the neutral stability point will lead to either sheet collapse or radial sheet blowout.

For a swirling annular sheet with inertia and surface tension only, energy is conserved with energy exchange between potential (surface) energy and kinetic energy (due to angular and radial momentum). However, with an imposed pressure difference, energy exchange with the ambient gas takes place, which might render the sheet unstable. For the latter case, one should note the similarity to the observations for a steady-state spatially developing free falling liquid curtain with a pressure difference across the sheet made by Finnicum et al. (1993) for the planar case and by Ramos (1997b) for the axisymmetric annular case.

Similarly to the prescribed oscillatory behavior of cylindrical liquid layers with excess swirl, the spatial development of annular sheets exiting from a nozzle or atomizer with excess swirl, is characterized by sheet divergence close to the nozzle exit and, if sheet break-up does not occur, subsequent oscillatory variations of the annular radius in the downstream direction. With regard to the diverging part of the sheet directly at the nozzle exit, we subsequently present a spatial analysis of swirling 'conical' sheets.

Further details on the analysis of film blowing under various conditions and for inviscid and viscous liquid layers can be found in the book by Yarin (1993). The stability analysis of periodically disturbed infinite annular sheets subject to film blowing (i.e. uniform radial sheet expansion) is another interesting problem which might provide some insight with regard to the influence of sheet attenuation on sheet stability. Although such an analysis is not presented here, it

is expected that, for large Weber numbers or large sheet velocities, similar results will be observed as for the modulated semi-infinite conical sheets analyzed below.

3.3. "Conical sheets" / steady-state analysis

Steady-state nonlinear solutions for the pure boundary-value problem of a swirling annular film exiting from a nozzle or atomizer have been obtained for various sets of boundary conditions at the nozzle exit and by employing a fourth-order Runge–Kutta integrator for a system of ordinary differential equations governing Δr, $\bar{r}$ and their spatial derivatives in z.

Neglecting the time-dependence in Eqs. (8) and (11) and employing the kinematic condition Eq. (12), i.e., $\mathrm{d}\bar{r}/\mathrm{d}z = \overline{v_r}/\overline{v_z}$, the conservation of mass and the conservation of angular momentum are given by

$$\Delta r \bar{r}\,\overline{v_z} = c_1,$$
$$\bar{r}\,\overline{v_\theta} = c_2,$$

where c_1 and c_2 are proportional to the constant mass flow rate and the constant angular momentum, respectively. Using the prescribed kinematic condition and the above equations to express $\overline{v_z}, \overline{v_r}$ and $\overline{v_\theta}$ in Eqs. (9) and (10) (with $\partial(\ldots)/\partial z = 0$ and Δp and $\bar{p}$ expressed by Eqs. (13)–(16)), the following system of first-order ordinary differential equations can be formulated:

$$\frac{\mathrm{d}\bar{r}^*}{\mathrm{d}z^*} = s, \tag{26}$$

$$\frac{\mathrm{d}s}{\mathrm{d}z^*} = \frac{\mathrm{d}^2\bar{r}^*}{\mathrm{d}z^{*2}} = t, \tag{27}$$

$$\frac{\mathrm{d}\Delta r^*}{\mathrm{d}z^*} = f, \tag{28}$$

$$\frac{\mathrm{d}f}{\mathrm{d}z^*} = \frac{\mathrm{d}^2\Delta r^*}{\mathrm{d}z^{*2}} = g \tag{29}$$

and

$$\begin{bmatrix} \mathrm{d}g/\mathrm{d}z^* \\ \mathrm{d}t/\mathrm{d}z^* \end{bmatrix} = \begin{bmatrix} A_{11} & A_{12} \\ A_{21} & A_{22} \end{bmatrix}^{-1} \begin{bmatrix} K_1 \\ K_2 \end{bmatrix}, \tag{30}$$

where

$$A_{11} = p/2,$$
$$A_{12} = m,$$
$$A_{21} = -\varepsilon^2 m/\Delta r^*,$$
$$A_{22} = \frac{c_1^2}{(\bar{r}^*\Delta r)^2} - 2\varepsilon^2 p/\Delta r^*,$$

$$
\begin{aligned}
K_1 = & -\frac{1}{\varepsilon^2}\left(\frac{c_1}{\Delta r^* \bar{r}^*}\right)^2\left[\frac{s}{\bar{r}^*}+\frac{f}{\Delta r^*}\right] - \left\{\frac{\Delta p}{2}g + \Delta m t \right. \\
& + C^{-1}\left(\frac{q}{2}f - ns + \frac{\Delta q}{2}\Delta r^* - \Delta m \bar{r}^*\right) \\
& \left. - C^{-2}\left(\frac{q}{2}\Delta r^* - n\bar{r}^*\right)\left[2\bar{r}^* s - \frac{\Delta r}{2}f\right]\right\} \\
& + 2\left\{pt + \frac{m}{2}g - C^{-1}\left(q\bar{r}^* - \frac{m}{2}\Delta r^*\right)\right\}\left(\frac{s}{\Delta r^*}+\frac{f}{4\bar{r}^*}\right), \\
K_2 = & \, 2\varepsilon^2\left\{\left(-\frac{f}{\Delta r^{*2}}\right)\left(pt + \frac{m}{2}g - C^{-1}\left(q\bar{r}^* - \frac{m}{2}\Delta r^*\right)\right)\right. \\
& + \frac{1}{\Delta r^*}\left[\Delta p t + \frac{\Delta m}{2}g - C^{-1}\left(qs - \frac{n}{2}f + \Delta q \bar{r}^* - \frac{\Delta n}{2}\Delta r^*\right)\right. \\
& \left.\left. + C^{-2}\left(q\bar{r}^* - \frac{m}{2}\Delta r^*\right)\left(2\bar{r}^* s - \frac{\Delta r^*}{2}f\right)\right]\right\} \\
& + c_1^2\left\{\frac{2}{\left(\bar{r}^*\Delta r^*\right)^3}(\Delta r^* s + \bar{r}^* f)t \right. \\
& - \left[\frac{2}{\left(\bar{r}^*\Delta r^*\right)^3}(\Delta r^* s + \bar{r}^* f)s - \frac{1}{\left(\bar{r}^*\Delta r^*\right)^2}t\right]\left[\frac{s}{\bar{r}^*}+\frac{f}{\Delta r^*}\right] \\
& \left. + \frac{1}{\left(\bar{r}^*\Delta r^*\right)^2}s\left[-\frac{s^2}{\bar{r}^{*2}} + \frac{t}{\bar{r}^*} - \frac{f^2}{\Delta r^{*2}} + \frac{g}{\Delta r^*}\right]\right\} - 3\frac{c_2^2}{\bar{r}^{*4}}s
\end{aligned}
$$

with $p = G_+ + G_-$, $m = G_+ - G_-$, $q = F_+ + F_-$, $n = F_+ - F_-$, $\Delta p = \mathrm{d}(G_+ + G_-)/\mathrm{d}z^*$, $\Delta m = \mathrm{d}(G_+ - G_-)/\mathrm{d}z^*$, $\Delta q = \mathrm{d}(F_+ + F_-)/\mathrm{d}z^*$, and $\Delta n = \mathrm{d}(F_+ - F_-)/\mathrm{d}z^*$. If $G_\pm = F_\pm = 1$ is assumed, an equation for $\mathrm{d}t/\mathrm{d}z^*$ does not have to be solved. In this case $\mathrm{d}s/\mathrm{d}z^*$ and $\mathrm{d}g/\mathrm{d}z^*$ are given by

$$
\begin{aligned}
\mathrm{d}s/\mathrm{d}z^* = & \left(\frac{c_1^2}{\left(\bar{r}^*\Delta r^*\right)^2} - \frac{4\varepsilon^2}{\Delta r^*}\right)^{-1}\left[\frac{c_2^2}{\bar{r}^{*3}} - 4\varepsilon^2\frac{1}{\Delta r^*}\frac{\bar{r}^*}{\bar{r}^{*2} - \Delta r^{*2}/4}\right. \\
& \left. + c_1^2\frac{1}{\left(\bar{r}^*\Delta r^*\right)^2}\left(\frac{s}{\bar{r}^*}+\frac{f}{\Delta r^*}\right)s\right], \\
\mathrm{d}g/\mathrm{d}z^* = & -\frac{1}{\bar{r}^{*2} - \Delta r^{*2}/4}f + \frac{\Delta r^*}{\left(\bar{r}^{*2} - \Delta r^{*2}/4\right)^2}\left(2\bar{r}^* s - \frac{1}{2}\Delta r^* f\right) \\
& + 4\left[\mathrm{d}s/\mathrm{d}z^* - \frac{\bar{r}^*}{\bar{r}^{*2} - \Delta r^{*2}/4}\right]\left[\frac{s}{\Delta r^*}+\frac{f}{4\bar{r}^*}\right] \\
& - \frac{c_1^2}{\varepsilon^2}\frac{1}{\left(\bar{r}^*\Delta r^*\right)^2}\left[\frac{s}{\bar{r}^*}+\frac{f}{\Delta r^*}\right].
\end{aligned}
$$

Clearly, assuming $G_{\pm} = 1$ reduces the order of the highest spatial derivative of $\bar{r}$ in Eq. (9) from three to two. Note that the pressure term $-1/\rho_l \partial\bar{p}/\partial z)$ appearing on the right-hand side of Eq. (9) is obtained from Eq. (13) where $\partial^2\bar{r}/\partial z^2$ disappears if $G_{\pm} = 1$ is assumed.

For the general case ($G_{\pm} \neq 1$, $F_{\pm} \neq 1$), boundary conditions were specified for the nondimensional sheet thickness $\Delta r^* = b_1$ and the nondimensional radial distance of the sheet centerline from the axis of symmetry $\bar{r}^* = b_4$ as well as their first and second spatial derivatives ($\mathrm{d}\Delta r^*/\mathrm{d}z^* = b_2$, $\mathrm{d}^2\Delta r^*/\mathrm{d}z^{*2} = b_3$, $\mathrm{d}\bar{r}^*/\mathrm{d}z^* = b_5$, $\mathrm{d}^2\bar{r}^*/\mathrm{d}z^{*2} = b_6$) at the nozzle exit. For the simplified case with $G_{\pm} = F_{\pm} = 1$, a boundary condition for $\mathrm{d}^2\bar{r}^*/\mathrm{d}z^{*2}|_{z^*=0}$ is not required due to the prescribed reduction of the highest-order spatial derivative in $\bar{r}^*$ in this case. For the general case, the boundary condition for $\mathrm{d}^2\bar{r}^*/\mathrm{d}z^{*2}$ at $z^* = 0$ was specified to take the value obtained from the corresponding simplified analysis (with $G_{\pm} = F_{\pm} = 1$).

To solve the general and simplified steady-state problem, the axial and circumferential velocity components ($\overline{v_{z,0}}$ and $\overline{v_{\theta,0}}$) or alternatively the mass flow rate (i.e., $\overline{v_{z,0}}\Delta r_0\bar{r}_0$) and the swirl at the nozzle exit (i.e., $\overline{v_{\theta,0}}\bar{r}$) also had to be specified.

This implies that eight boundary conditions are to be specified at the nozzle exit, if the general steady-state problem is to be solved by integrating the above system of ODEs for increasing values of z^* starting from the nozzle exit at $z^* = 0$. Similar steady-state analyses were also presented by Yarin (1993) for the case of swirling liquid membranes and by Ramos (1992) for nonswirling thin liquid sheets. As within the prescribed analysis, the latter authors specified boundary conditions only at the location where the sheet exits the nozzle or atomizer.

It is emphasized here that, in general, boundary conditions should not only be specified at the nozzle exit. In fact, the number of boundary conditions to be prescribed at the inflow and outflow planes of the considered spatial domain will depend, in analogy to the consideration and rejection of certain wavenumbers within the previous section, on the group velocities or energy propagation characteristics associated with the (capillary) waves travelling along the sheet. A more detailed description regarding the specification of boundary conditions and selection of relevant wavenumbers by means of group velocity arguments of the possible wave systems can be found elsewhere (Mehring and Sirignano, 1999, 2000b).

Clearly, nonlinear steady-state solutions obtained by specification of boundary conditions at the upstream boundary only are not guaranteed to reflect accurately the physical problem at hand. Nevertheless, it can be shown that for the cases presented here, the solutions to the nonlinear steady-state problem with boundary conditions at the nozzle exit only, provide 'reasonable' initial-conditions for the analysis of steady-state diverging sheets with superimposed unsteady modulations enforced at the nozzle exit. Also, referring to the work by Entov et al. (1980), Yarin (1993) noted that the effect of boundary conditions at the far end of a viscous liquid film appears to a great extent only in a narrow boundary layer and does not propagate upstream for fairly large Reynolds numbers.

Nonlinear numerical solutions of the unsteady equations (as described later) using the prescribed steady-state solutions as initial conditions showed that, for larger Weber numbers, the prescribed steady-state solutions are in fact time-independent and stable with regard to disturbances generated by numerical error. For the lower Weber number range, small-amplitude short-wavelength disturbances were found within the steady-state solution for the axial velocity of the diverging sheet near the nozzle exit. In the corresponding numerical solution of the unsteady problem, these disturbances are propagated downstream at decreasing amplitudes. The solution

relaxes towards a truly steady state with spatial variations of $\Delta r, \overline{r}, \overline{u}, \overline{v}$ and $\overline{w}$ very close to the predicted steady-state solution but without oscillations in $\overline{u}$.

Also, for large Weber number values, transient numerical simulations of the nonlinear unsteady problem given by an initially annular swirl-stabilized sheet with gradually increasing swirl at the nozzle exit (towards a fixed value) provided the same steady-state solutions near the orifice as those obtained by solution of the corresponding steady-state problem. For smaller Weber numbers, oscillations in $\overline{u}$ predicted by the steady-state solutions do not appear in the quasi-steady-state solutions observed within the transient simulations and at the nozzle exit. However, the latter agree with the truly time-independent solutions obtained from nonlinear numerical simulations using the 'steady-state' solutions obtained from Eqs. (26)–(30) as initial conditions.

Fig. 4(a)–(d) illustrate solutions to the nonlinear steady-state problem for various boundary conditions. For the cases with $b_2 = b_3 = b_5 = 0$, the radial distance of the film from the axis of symmetry decreases monotonically resulting in sheet collapse if the angular momentum at the nozzle exit is smaller than the amount needed to stabilize the undisturbed annular sheet with radius $\overline{r_0}$ and thickness Δr_0. In this case, the centrifugal forces cannot compensate for the capillary pressure which acts towards a minimization of the surface area of the swirling film. If the angular velocity at the nozzle exit exceeds the critical value which stabilizes the annular configuration, i.e.,

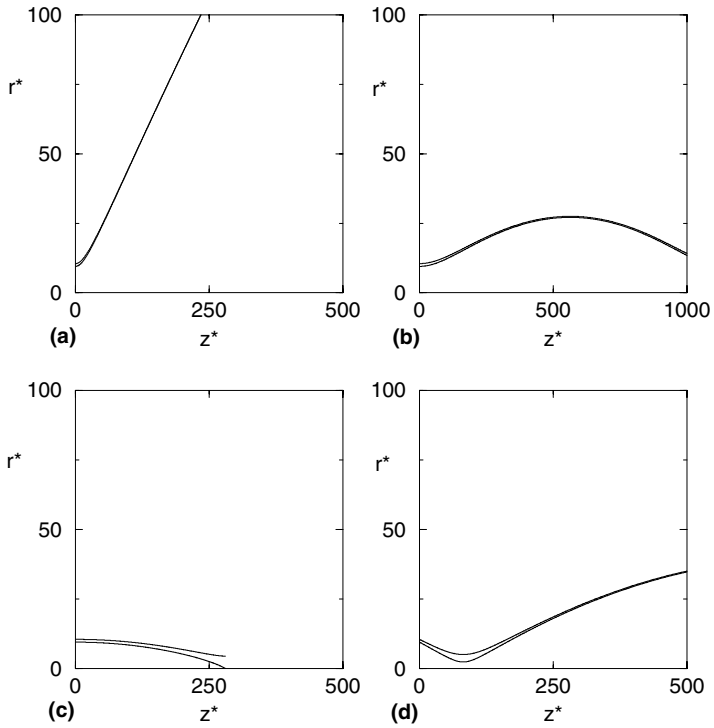

Fig. 4. Steady-state solutions for $We = 1000$, $b_1 = 1, b_2 = b_3 = 0, b_4 = 10$ and $b_5 = 0$ (cases a–c) or $b_5 = -0.1$ (case d) $[G_\pm = F_\pm = 1]$. The nondimensional mass flow rate is $c_1 = \overline{r}_0^*$ and the nondimensional angular momentum is $c_2 = kc_{2,0}$, where $c_{2,0}$ corresponds to the amount of swirl required to stabilize the undisturbed annular sheet, i.e., $c_{2,0} = \overline{r}_0^* \overline{v}_{\theta,0}^*$: (a) $k = 10$, (b) $k = 2$, (c) $k = 0.1$ and (d) $k = 1$.

$\overline{v_\theta}^*_{,0} = \sqrt{2/[We(1-\Delta r_0^2/(4\bar{r}_0^2))]}$, the radial centerline-position of the film undulates in the downstream direction of the nozzle according to the energy transfer between surface energy and energy stored within the swirling motion of the sheet. These sheets are often described as 'conical' in the engineering practice although they can deviate substantially from a true conical shape.

3.4. Swirling annular and "conical" sheets modulated at the nozzle exit

Nonlinear unsteady numerical solutions for thin swirling annular or 'conical' liquid sheets, with or without harmonic sinuous or dilational modulations enforced at the nozzle exit, have been obtained by using the 'angled-derivative' scheme described by Richtmyer and Morton (1967). Only larger Weber number cases (i.e., $We \gg 2$) are considered, as transient effects are found to dominate the distortion and sheet break-up process at lower Weber number values. The latter has already been observed within the analysis of pressure-stabilized annular sheets (Mehring and Sirignano, 2000b).

In the "inviscid" simulations presented here, small amounts of viscosity were included in order to prevent the development of finite-time singularities within the inviscid reduced-dimension analysis ('inviscid-slice model'). A detailed discussion/description of this phenomenon, the included viscous term, and the limitations of a pure inviscid model have already been provided by Mehring and Sirignano (2000a,b) using the same numerical model. These references also include a review of previous work on liquid sheets considering the effects of liquid viscosity.

Initial conditions for the numerical simulations were chosen according to the steady-state solution illustrated in Fig. 4(a) or the similar case, but with exactly enough swirl to stabilize the sheet in its annular configuration as it exits from the nozzle.

For both swirl-stabilized annular and 'conical' sheets, the number of boundary conditions at the nozzle exit was chosen according to the number of wavenumbers l_i or k_i with associated positive group velocities, relevant to the linear boundary-value problem analysis presented earlier for swirl-stabilized annular sheets. Boundary conditions at the nozzle exit for nondimensional sheet thickness Δr^*, radial sheet-centerline location $\bar{r}^*$, and the velocity components in the axial, radial and circumferential direction were chosen according to the prescribed steady-state solutions, but with additional harmonic variations of the axial or transverse velocity components according to $\overline{v}^*_{z,r} = A_{z,r}[1-\mathrm{e}^{-t^*/T_\mathrm{s}}]\sin(2\pi t^*/T_\mathrm{p}+\alpha)$, where T_p is the nondimensional time-period of the harmonic forcing and A_z and A_r denote the nondimensional amplitudes of the axial or transverse velocity modulation, respectively; the superscript '*' denotes a nondimensional quantity.

Additional numerical boundary conditions required to solve the unsteady problem were specified for $\partial^2\Delta r^*/\partial z^{*2}$ and $\partial^2\bar{r}^*/\partial z^{*2}$ with values corresponding to the imposed steady-state initial conditions. Note however that the use of $\partial^4\Delta r^*/\partial z^{*4}=0$ and $\partial^4\bar{r}^*/\partial z^{*4}=0$ at $z^*=0$ (already employed as numerical conditions within the analysis of pressure-stabilized annular sheets) instead of the prescribed second-order derivatives, does not yield significant differences within the solution of the transient problem with steady-state limit-cycle solution; the latter being analyzed in connection with the steady-state problem described in the previous section.

In summary, for the analysis of the considered unsteady problem, 5 boundary conditions and 2 numerical conditions were specified at the nozzle exit, whereby the specification of $\bar{v}$ effectively determines $\partial\bar{r}^*/\partial z^*$ in the steady-state case without sheet modulation. Within the solution of the

unsteady equations, a boundary condition for $\partial\Delta r^*/\partial z^*$ (as specified within the steady-state analysis of the previous section) was not imposed; however, numerical simulations show that in the unsteady transient simulations with steady-state limit-cycle solution, $\partial\overline{v}_z^*/\partial z^*|_{z^*=0} = 0$ and $\partial\Delta r^*/\partial z^*|_{z^*=0} = -\partial\overline{r}^*/\partial z^*|_{z^*=0} = 0$ as expected from analytical solution to the corresponding steady-state problem.

Figs. 5 and 6 compare swirling annular and conical sheets subjected to the same dilational (Fig. 5) or sinuous (Fig. 6) modulation at the nozzle exit. Both cases illustrate how sheet thinning in the conical case yields longer break-up lengths compared to the corresponding annular cases (with only enough swirl to maintain the annular geometry). Sheet divergence results in larger liquid surface area, implying that energy density of the disturbance imposed onto the sheet becomes smaller in the diverging case. Consequently, absolute disturbance amplitudes downstream from the nozzle are smaller in the diverging case. The characteristics of the nonlinear distortion of sinusoidally or dilationally modulated swirling axisymmetric annular sheets with fluid agglomeration into rings and thin shells connecting them is not fundamentally altered by the thinning of

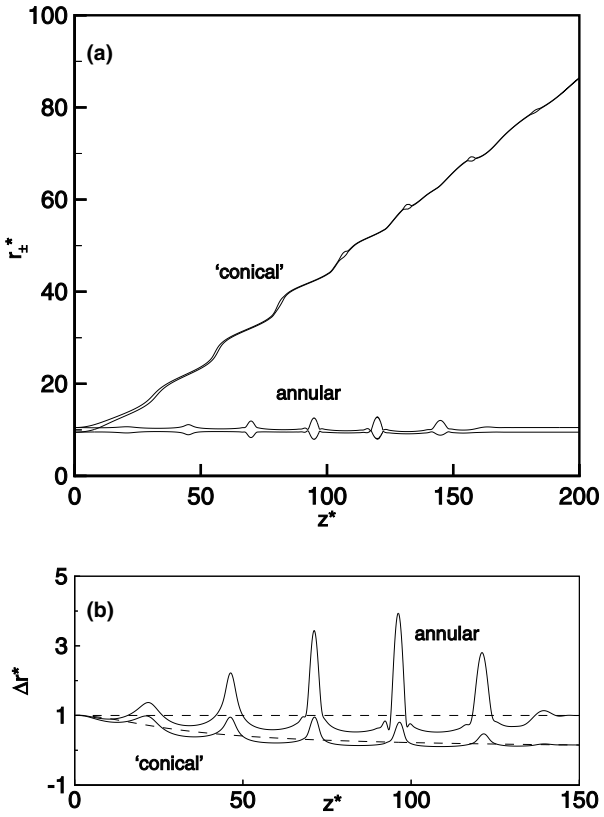

Fig. 5. Annular and "conical" liquid films dilationally modulated at the nozzle exit [$G_\pm = F_\pm = 1$]. Initial conditions are the steady-state solutions $(- - -)$ for $We = 1000, b1 = 1, b_2 = b_3 = b_5 = 0, b_4 = 10$ with angular momentum $c_2 = k\overline{r}_0^*\overline{v}_{\theta,0}^*$ and $k = 1$ (annular case) or $k = 10$ ("conical" case). The modulation is specified by $A_z = 0.05$ and $T_p = 25$. Solutions are displayed at: (a) $t^* = 200$ ("conical" case), $t^* = T_b = 163.69$ (annular case), and (b) $t^* = 140$.

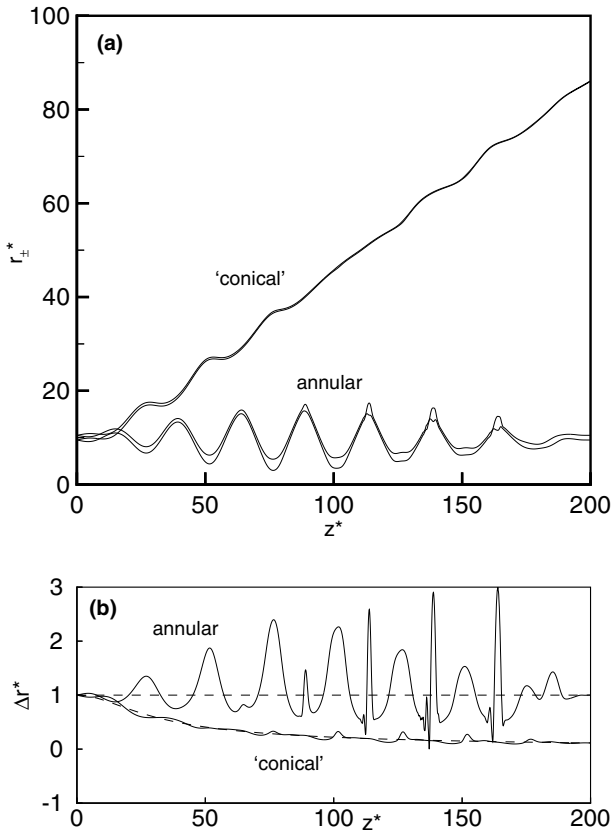

Fig. 6. Annular and "conical" liquid films sinusoidally modulated at the nozzle exit [$G_{\pm} = F_{\pm} = 1$]. Initial conditions are the steady-state solutions ($- - -$) for $We = 1000, b1 = 1, b_2 = b_3 = b_5 = 0, b_4 = 10$ with angular momentum $c_2 = k\overline{r}_0^*\overline{v}_{\theta,0}^*$ and $k = 1$ (annular case) or $k = 10$ ("conical" case). The modulation is specified by $A_r = 0.1$ and $T_p = 25$. Solutions are displayed at $t^* = 200$ ("conical" case) and $t^* = T_b = 188.98$ (annular case).

the sheet in the 'conical' case. This is particularly true for the dilationally modulated sheet illustrated in Fig. 5. It should be noted however, that in the 'conical' case of Fig. 5 sheet divergence and sheet thinning cause stronger coupling between the modulated dilational and excited sinuous mode (causing larger sinuous sheet disturbances) than in the corresponding annular case. For the case with modulations of the transverse velocity component (Fig. 6), higher harmonics are observed in the annular case, whereas in the similar case with excess swirl (i.e., 'conical' case), these harmonics do not appear on the diverging sheet. Sheet divergence is found to significantly influence breakup times and breakup lengths. For the dilationally and sinusoidally modulated swirling (nondiverging) annular sheets depicted in Figs. 5 and 6, sheet breakup occurred at $T_b = 163.69$ and $T_b = 188.98$ with breakup lengths $l_b = 117.36$ and $l_b = 137.2$, respectively. For the similar case with excess swirl, resulting in a diverging sheet with monotonically decaying sheet thickness in the steady solution, sheet breakup was not observed for $t^* < 200$.

Sheet divergence, breakup time and breakup length for the general case with $G_{\pm} \neq 1$ vary slightly from those obtained for the case illustrated in Figs. 5 and 6 with $G_{\pm} = 1$. However, the

prescribed characteristics of the nonlinear sheet distortion due to sinuous or dilational modulations are valid independently of the assumptions employed for $G_{\pm}$.

Sheet thinning (produced by excess swirl) results (for sinuous modulations) in a weaker coupling of sinuous and dilational modes (Fig. 6) and (for sinuous or dilational modulations) in a delay of the appearance of higher harmonic dilational waves which lead to local sheet pinch-off (Figs. 5 and 6). It is agreed here that the shortest of the produced wavelengths cannot be accurately predicted by the employed model. Nevertheless, it is claimed, and it has already been shown for planar sheets (Mehring and Sirignano, 1999), that the evolution of the sheet until pinch-off (including some higher-harmonic effects) is properly predicted qualitatively and quantitatively within some margin of error.

Parametric studies on the effect of Weber number, swirl number [5] and disturbance amplitudes $A_{r,z}$ on break-up time and break-up length of dilationally and sinuous modulated annular or 'conical' sheets have been conducted for the general case with $G_{\pm} \neq 1$ and for sheets with $\bar{r}^* = 10$ at the nozzle exit, Weber numbers $We = 150$, 500, 1000, or 2000 and swirl numbers $k = 1, 5, 10, 20$. The following four base cases were considered:

1. $We = 1000, k = 1, A_z = 0.025, A_r = 0, T_p = 15, T_s = T_p/4, \alpha = 0$,
2. $We = 1000, k = 1, A_z = 0.02, A_r = 0, T_p = 100, T_s = T_p/4, \alpha = 0$,
3. $We = 1000, k = 1, A_z = 0, A_r = 0.1, T_p = 25, T_s = T_p/4, \alpha = \pi/2$, and
4. $We = 1000, k = 1, A_z = 0, A_r = 0.1, T_p = 100, T_s = T_p/16, \alpha = \pi/2$.

Cases 1 and 2 correspond to dilational modulations which result, according to the prescribed linear analysis, in unstable sheet behavior. Cases 3 and 4 correspond to configurations already considered in the analysis of pressure-stablized annular sheets with sinuous modulations enforced at the nozzle, where they resulted in stable and unstable sheet behavior, respectively. Note that according to the linear analysis presented earlier, and within the parameter range of interest, swirl-stabilized annular sheets with sinuous modulations enforced at the orifice are stable, as long as $We < 2$ (approximately).

Tables 1–5 show the results of the parametric studies on Weber number and swirl number for the case with $G_{\pm} \neq 1$ and $F_{\pm} \neq 1$. Depicted are break-up lengths l_b and break-up times t_b for the four base cases 1–4 and their variations which are obtained by changes in Weber number and/or swirl number. Each table also illustrates the break-up length and time for a planar sheet [6] with the same swirl number and modulation enforced at the nozzle as for the corresponding base case.

Steady-state solutions and transient simulations for time-independent conditions at the nozzle exit showed that higher swirl numbers k result in larger cone-angles and an increase in the thinning rate of the sheet in the downstream direction. The analysis of sheets which are modulated at the nozzle exit showed that an increase in the thinning rate results in smaller absolute amplitude disturbances downstream for the same amplitude at the nozzle. Consequently, the appearance of nonlinear effects (i.e., higher harmonic disturbances) is (in general) delayed resulting in longer

[5] Here, the term 'swirl number' refers to the ratio k of swirl c_2 imposed at the nozzle exit to the amount of swirl $c_{2,0}$ necessary to stabilize the sheet in its annular configuration, i.e. $c_2 = kc_{2,0}$.

[6] Planar sheets are approximated here by swirl-stabilized annular sheets with an annular radius $\bar{r}^* = 10^4$ at $z^* = 0$.

Table 1
Swirl-stabilized annular ($k = 1$) and 'conical' ($k = 10, 20$) sheets with modulations of the axial velocity component at the nozzle exit, i.e., $\overline{v_z}^* = A_z[1 - e^{-t^*/T_s}]\sin(2\pi t^*/T_p + \alpha)$, for various Weber numbers We; $R = 10, A_z = 0.025, T_p = 15$, $T_s = T_p/4, \alpha = 0$; t_b, l_b = nonlinear break-up time and length; 'planar' refers to a case with very large radius of curvature (i.e., $R = 10^4, k = 1$) and with the same modulation enforced at $z^* = 0$; base case 1

	Planar	$k = 1$	$k = 10$	$k = 20$
$We = 150$				
t_b		171.1		
l_b		151.5		
$We = 500$				
t_b	175.6	181.3	221.5	304.2
l_b	156.4	162.7	208.2	284.6
$We = 1000$				
t_b	164.3	170.2	180.3	277.1
l_b	146.1	152.1	164.2	264.7
$We = 2000$				
t_b	154.2	155.1	163.5	210.0
l_b	136.7	137.7	146.8	194.3

Table 2
Swirl-stabilized annular ($k = 1$) and 'conical' ($k = 5, 10$) sheets with modulations of the axial velocity component at the nozzle exit, i.e., $\overline{v_z}^* = A_z[1 - e^{-t^*/T_s}]\sin(2\pi t^*/T_p + \alpha)$, for various Weber numbers We; $R = 10, A_z = 0.02, T_p = 100$, $T_s = T_p/4, \alpha = 0$; t_b, l_b = nonlinear break-up time and length; 'planar' refers to a case with very large radius of curvature (i.e., $R = 10^4, k = 1$) and with the same modulation enforced at $z^* = 0$; 'nb' indicates no break-up within the simulated time frame ($0 < t^* < 1050$); base case 2

	Planar	$k = 1$	$k = 5$	$k = 10$
$We = 500$				
t_b	1025.7	768.4	783.0	nb
l_b	917.6	664.2	698.9	
$We = 1000$				
t_b	1012.1	852.4	830.0	976.6
l_b	905.3	748.4	735.2	902.0
$We = 2000$				
t_b	1002.9	905.6	870.5	938.2
l_b	897.6	801.6	770.9	845.0

break-up times and larger break-up lengths. Tables 1–5 show that this is particularly true for sinuous modulated sheets (i.e. modulation of the transverse velocity at the nozzle exit). Also, for large enough thinning rates (i.e. swirl numbers), sheet break-up might not occur, even though break-up was predicted at lower thinning rates under the same forcing conditions. The prescribed effect of sheet divergence or swirl-number on break-up lengths and times has been observed for all the considered Weber numbers, i.e. $We = 500, 1000$ and 2000. 'Conical' sheets with lower Weber number values have not been analyzed due to small-amplitude short-wavelength oscillations within the corresponding steady-state solutions (as described earlier) used as initial conditions for the transient simulations.

Table 3
Swirl-stabilized annular ($k = 1$) and 'conical' ($k = 10, 20$) sheets with modulations of the transverse velocity component at the nozzle exit, i.e., $\overline{v_r}^* = A_r[1 - e^{-t^*/T_s}]\sin(2\pi t^*/T_p + \alpha)$, for various Weber numbers We; $R = 10, A_r = 0.1, T_p = 25$, $T_s = T_p/4, \alpha = \pi/2$; t_b, l_b = nonlinear break-up time and length; 'planar' refers to a case with very large radius of curvature (i.e., $R = 10^4, k = 1$) and with the same modulation enforced at $z^* = 0$; 'nb' indicates no break-up within the simulated time frame ($0 < t^* < 550$); base case 3

	Planar	$k = 1$	$k = 10$	$k = 20$
$We = 150$				
t_b		115.5		
l_b		87.8		
$We = 500$				
t_b	157.5	131.8	534.7	nb
l_b	130.3	105.1	476.4	
$We = 1000$				
t_b	175.1	146.3	297.7	nb
l_b	160.3	119.8	273.0	
$We = 2000$				
t_b	196.7	163.7	227.2	nb
l_b	182.1	137.3	201.8	

Table 4
Swirl-stabilized annular ($k = 1$) and 'conical' ($k = 10, 20$) sheets with modulations of the transverse velocity component at the nozzle exit, i.e., $\overline{v_r}^* = A_r[1 - e^{-t^*/T_s}]\sin(2\pi t^*/T_p + \alpha)$, for various Weber numbers We; $R = 10, A_r = 0.1, T_p = 100$, $T_s = T_p/16, \alpha = \pi/2$; t_b, l_b = nonlinear break-up time and length; 'planar' refers to a case with very large radius of curvature (i.e., $R = 10^4, k = 1$) and with the same modulation enforced at $z^* = 0$; 'nb' indicates no break-up within the simulated time frame ($0 < t^* < 600$); base case 4

	Planar	$k = 1$	$k = 10$	$k = 20$
$We = 500$				
t_b	494.1	313.3	nb	nb
l_b	479.4	299.4		
$We = 1000$				
t_b	437.9	320.3	nb	nb
l_b	423.4	307.1		
$We = 2000$				
t_b	434.8	332.3	nb	nb
l_b	421.0	319.8		

The simulations illustrated in Tables 1–4 also showed that break-up lengths and times for swirl-stabilized modulated annular sheets are (with the exception of base case 1) smaller than those predicted for the corresponding planar cases. On the other hand, break-up lengths and times for similar diverging sheets (with excess swirl at the nozzle exit) are generally (i.e., with the exception of base case 2) significantly greater than for the planar case. This is found to be particularly true for larger swirl numbers k and sinuous mode simulations.

We shall now address the effects of Weber number on break-up length and time for the cases illustrated in Tables 1–4. For dilational sheet modulations, the effect of Weber number changes on l_b and t_b is determined by the relative importance of the radius of curvature in the main flow direction R_1 and the radius of curvature in the corresponding perpendicular direction R_2.

Table 5
Swirl-stabilized annular ($k = 1$) and 'conical' ($k = 10, 20$) sheets with modulations of the transverse velocity component at the nozzle exit, i.e., $\overline{v_r}^* = A_r[1 - e^{-t^*/T_s}]\sin(2\pi t^*/T_p + \alpha)$, for two forcing periods T_p; $We = 1000, R = 10, A_r = 0.5, T_s = T_p/4$ or $T_p/16, \alpha = \pi/2$

	$k = 1$[a]	$k = 10$[b]	$k = 20$[b]
$T_p = 25$			
$t_{b,c}$	30.8	69.1	79.5
$l_{b,c}$	18.6	65.1	55.1
$T_p = 100$			
$t_{b,c}$	59.6	127.4	341.7
$l_{b,c}$	19.9	118.1	344.4

[a] Sheet collapse where t_c and l_c are the nonlinear collapse time and length.
[b] Sheet break-up where t_b and l_b are the nonlinear break-up time and length.

By linear analysis, capillary effects on swirl-stabilized annular sheets resulting from R_1 are stabilizing whereas those resulting from R_2 are destabilizing to the sheet. This implies that, for $R_2 \gg R_1$ increasing *We* leads to smaller (stabilizing) surface tension forces and larger disturbance amplitudes generated by the enforced sheet modulation. This can be observed for the planar, annular and 'conical' cases presented in Table 1, where increasing Weber number values results in a decrease of break-up length l_b. The same arguments can also be used to explain the decrease in l_b with increasing *We*-values for planar and diverging 'conical' (i.e., $k = 10$) sheets illustrated in Table 2. However, for the annular case and the 'conical' case with $k = 5$ (i.e., only slightly diverging sheet) shown in Table 2, $R_2 \ll R_1$ along the sheet so that the destabilizing capillary effects associated with R_2 dominate, leading to an increase in l_b with an increase in Weber number *We*. The described behavior is not only a result of the relative importance of R_1 and R_2 but also due to a decrease in the thinning rate of the sheet if *We* is increased and k is kept constant. As pointed out earlier, increased sheet thinning results in larger break-up times and lengths if the same modulation is imposed at the nozzle exit.

For sinuous sheet modulations, sheet break-up occurs due to nonlinear coupling with the dilational mode. Here, the dependency of nonlinear breakup length and time on Weber number is greatly influenced by the linear and nonlinear mode coupling and the linear and nonlinear dilational mode behavior. The former decreases with increasing Weber number (and annular radius).

For long-wavelength sinuous mode disturbances on planar sheets (see Table 4), the dependency of l_b on *We* is dominated by the (long-wavelength) dilational mode distortion generated by the sinuous modulation, i.e. as *We* is increased, l_b decreases. For planar sheets with sinuous disturbances of shorter wavelength (see Table 3) and for the annular cases listed in Tables 3 and 4, the nonlinear coupling between the modulated sinuous and excited dilational mode dominates, leading to an increase in breakup length with increasing Weber number.

For diverging ('conical') sheets with low frequency sinuous modulations (see Table 3, $k = 10$), l_b decreases with an increase in *We*. The same observation has already been made for the dilationally modulated 'conical' sheets of Table 2 with $k = 10$ and can be attributed to a decrease in the thinning rate of the steady sheet resulting from an increase of *We* at the same swirl number k.

Increased sheet divergence leads to increased sheet thinning and smaller droplets once the thin ligaments detached from the sheet do disintegrate further (e.g. according to Rayleigh's mechanism for jet break-up). However, for purely capillary sheet break-up and diverging sheets, the increase

in the second radius of curvature and the prescribed decrease in disturbance amplitude renders the sheet more stable. This is in contrast to the case where aerodynamic effects dominate the sheet breakup. Here, sheet divergence leads to an increase in surface area onto which the surrounding gas can impose forces or transfer energy. Within the present analysis of capillary waves on diverging annular sheets, energy is only transferred onto the sheet at the nozzle exit.

The simulations presented here indicate that, in general, an increase in the thinning rate or cone-angle of diverging annular sheets resulting from an increase in the angular momentum or swirl at the nozzle exit, leads to smaller disturbance amplitudes and longer break-up lengths if the same modulation is forced onto the sheet at the nozzle exit. These break-up lengths and times might be significantly larger than those observed for the corresponding modulated planar sheets.

The effect of disturbance amplitudes A_r and A_v on break-up length l_b and break-up time t_b has also been investigated. The corresponding results illustrated in Table 6 indicate that an increase in the disturbance amplitude of the velocity modulation imposed at the nozzle exit will lead to a decrease of l_b and t_b for both sinuous and dilational modes.

Due to differences in the configuration, direct comparison of experimental data to the present results is not possible. For example, modulation at the nozzle exit has not been quantified and a precise description of the capillary wave behavior has not been given within prior experimental work. Swirling conical liquid sheets subjected to the effect of piezoelectric transducer modulation have been studied by Chung et al. (1998). However, for the case of interest, i.e. swirling conical sheets of low viscosity liquids in a gas of negligible density, no data was provided. Also, from the data provided by Chung et al. (1998), it is not known what precise waves were generated by the intrinsic disturbances generated by the pressure-swirl nozzle nor by the piezoelectric transducer whose sinusoidal input signal is known. (Note that, even when forcing the sheet harmonically at a single frequency multiple waves with different wavelengths will be generated.)

Apart from the presence of an ambient gas (whose effect might be negligible for small enough density ratios), previous experimental work on swirling conical sheets focused, in general, on droplet size distribution rather than sheet distortion characteristics before and up to break-up

Table 6
Swirl-stabilized 'conical' sheets with modulations of the transverse velocity component at the nozzle exit according to base cases 1–4; $We = 1000, R = 10, k = 10$; t_b, l_b = nonlinear break-up time and length; 'nb' indicates no break-up for $t^* < t_s$ (t_s = simulation time)

(1)	$A_z = 0.01$	$A_z = 0.025$	$A_z = 0.05$
t_b	$t^* < 400$	180.32	97.87
l_b	nb	164.17	81.45
(2)	$A_z = 0.01$	$A_z = 0.02$	$A_z = 0.05$
t_b	$t^* < 1200$	829.96	451.64
l_b	nb	735.15	351.30
(3)	$A_z = 0.05$	$A_z = 0.1$	$A_z = 0.25$
t_b	451.64	297.73	103.59
l_b	351.30	273.04	78.40
(4)	$A_z = 0.05$	$A_z = 0.1$	$A_z = 0.25$
t_b	$t^* < 600$	$t^* < 600$	464.11
l_b	nb	nb	461.36

(Ballester and Dopazo, 1996; Schmidt and Sojka, 1999). Clearly, whereas measurements of film locations, i.e. sheet centerline location, have been reported in the literature for various configurations other than the one analyzed here (Yarin, 1993; Kawano et al., 1997), measurements are currently not available for the instantaneous local thickness of the sheet even though current developments in diagnostic techniques are promising (Bachalo, 2000; Cousin et al., 2000). The knowledge of the thickness variation is essential to predict breakup. State-of-the-art measuring techniques do not allow comprehensive identification of the structure of swirling conical sheets. Such information was provided by the current investigation.

3.5. Swirl- and pressure-stabilized annular films

The nonlinear distortion and breakup of a nondiverging swirling annular liquid film with angular velocity $\overline{v_{\theta}}^{*}_{,0} = \sqrt{2/[We(1-\Delta r_0^2/(4\bar{r}_0^2))]}$ at the nozzle exit has been compared with the nonlinear breakup of the similar sheet but without swirl and stabilized (in its undisturbed annular configuration) with a constant gas-core pressure. The latter case has already been considered by the authors elsewhere (Mehring and Sirignano, 2000b). Both cases are unstable by linear analysis. Initial conditions for the case with swirl are given by the steady-state solution with boundary conditions $b_1 = 1, b_2 = 0, b_3 = 0, b_4 = 10, b_5 = 0$ and the prescribed angular velocity. The steady-state solution is independent of the mass flow rate in this case.

Fig. 7 illustrates both solutions at the time where sheet breakup occurs. The bubble formation observed for 'pressure-stabilized' nonswirling annular sheets (Mehring and Sirignano, 2000b), is

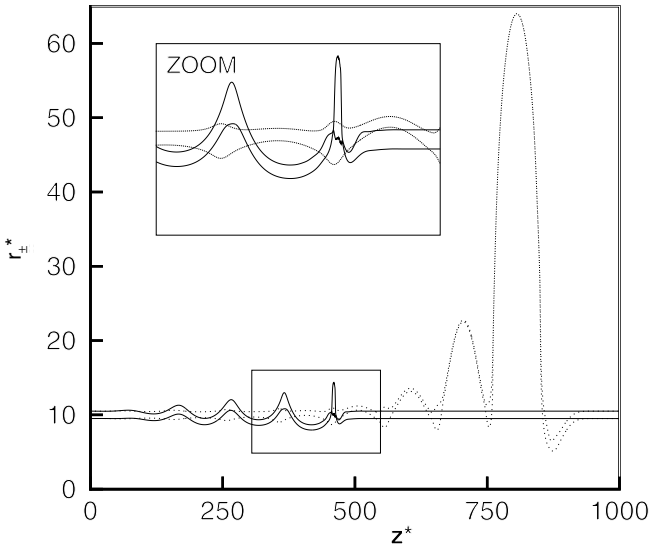

Fig. 7. Annular dilationally modulated nondiverging liquid film stabilized (in its undisturbed configuration) by a constant gas-core pressure and no swirl (dotted), or by a constant swirl but zero gas-core pressure (solid). The semi-infinite sheet is initially undisturbed [$We = 150, \bar{r}_0^* = 10, T_p = 100, A_z = 0.02$]. Solutions are displayed at time $t^* = T_b$ when breakup occurs, i.e., at $T_b = 465.1$ (swirl-stabilized case) and at $T_b = 856.6$ (pressure-stabilized case).

not observed for the 'swirl-stabilized' sheet. Also, as expected from linear analysis, sheet-breakup length and breakup times are considerably shorter in the case with swirl than in the case without swirl. For the swirling sheet, sheet breakup occurs at time $t^* = 465.1$ at a distance $z^* = 455.85$ from the nozzle exit. In the 'pressure-stabilized' case, sheet breakup occurs at $t^* = 856.6$ with a breakup length of $l_b = 849.45$.

3.6. Three-dimensional effects on swirling annular and conical films

The authors have completed three-dimensional simulations for two of the base cases (i.e. for swirling annular sheets) described above (i.e. base case 1 for dilational modulation and base case 3 for sinuous modulation) as well as for the corresponding conical configurations with swirl number $k = 10$.

Upon the original axisymmetric disturbances of the axial or transverse velocity components, circumferential disturbances were imposed in the same variable using a three-dimensional analysis and computational code. Modulations in the circumferential direction were specified in order to generate standing or travelling dilational or sinuous waves. The ratio between the amplitude of the axisymmetric disturbance and the superimposed three-dimensional modulation was varied between 0 and 1. For the traveling-wave case several different wave velocities were considered. Note that, sheet distortion is only predicted up to the point when the sheet thickness reaches zero at some location.

Distortion of the considered annular and conical sheets remained predominantly axisymmetric for cases where the ratio of the amplitude of the imposed circumferential disturbance to the axisymmetric disturbance amplitude was 0.1 and smaller. Even at a ratio 0.5, the characteristics of the sheet distortion remained essentially axisymmetric as shown in Fig. 8. If the amplitudes of axial and circumferential disturbance were comparable, sheet distortion was truly three-dimensional. The simulations also indicated that wave interaction between axial and circumferential waves is larger if the wave-velocities in the axial and circumferential direction are of the same order. Also, three-dimensional solutions for sheets with axisymmetric modulations only, remained axisymmetric throughout the simulations indicating that small perturbations due to numerical error did not result in a three-dimensional instability.

The observed dominance of the axisymmetric mode disturbance in these cases might be twofold. Firstly, the growth rate of excited unstable circumferential modes is too small to become important before the "large" amplitude axisymmetric sheet disturbances cause the sheet to break. Secondly, the excited circumferential modes are not unstable and the amplitudes of the waves in the circumferential direction remain moderate if no energy transfer from the axial waves occurs.

This investigation clearly indicates that there exists a domain in parameter space where predominantly axisymmetric modulations imposed at the nozzle exit will in fact result in a predominantly axisymmetric distorting sheet, with only minor effects of existing circumferential sheet disturbances. In fact, the prescribed situation is of practical interest, since hardware disturbances such as the axial dislocation of a swirl cup will generate an axisymmetric sheet modulation at the nozzle exit. Also, axial pressure fluctuations within the atomizer often might be considered to be uniform across the atomizer, leading to the generation of axisymmetric fluctuations in the axial fluid velocity which generates axisymmetric dilational distortions on the liquid sheet. The described observations only refer to the sheet distortion up to the point when the sheet ruptures

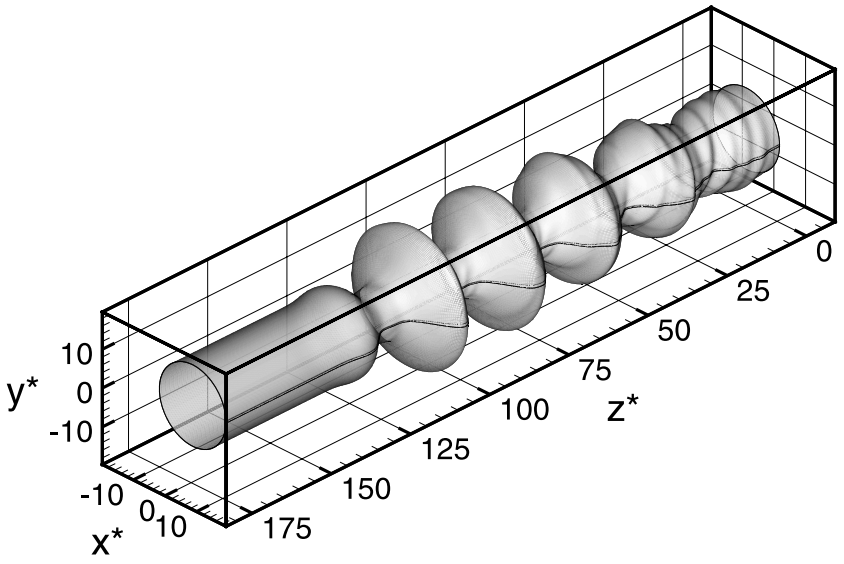

Fig. 8. Snap-shot of swirling annular liquid film sinusoidally modulated at the nozzle $z^* = 0$ according to base case 3 [$We = 1000, \bar{r}_0^* = 10, T_p = 25, A_r = 0.1, \alpha = \pi/2, T_s = T_p/4$] and with superimposed modulation of the transverse sheet velocity in the circumferential (θ^*-) direction, i.e. $\overline{v_r}^*(x^* = 0, \theta^*, t^*) = A_r[1 - e^{-t^*/T_s}] \sin(2\pi t^*/T_p + \alpha)\ [1 + 0.5\cos(3\theta^* - 2\pi t^*/T_{tr})]$ with $T_{tr} = 2\pi$ and $0 \leqslant \theta^* \leqslant 2\pi$. (Only the outer sheet interface is shown.)

locally for the first time. For harmonic three-dimensional modulations rupture might occur simultaneously at various points of the sheet at the same downstream distance. Contraction of the free rim(s) generated by the rupture(s) could be followed by more distinctly three-dimensional behavior.

4. Conclusions

A reduced dimension analysis is presented for the analysis of nonlinear dilational (symmetric) and sinuous (anti-symmetric) capillary waves on swirling axisymmetric thin inviscid liquid sheets exiting from a nozzle or atomizer into a void. New results obtained from the present analysis are the identification of the sheet distortion and breakup characteristics in the presence of sheet divergence due to swirl including the change of sheet breakup length.

Nonlinear solutions to the pure boundary-value problem with time-independent boundary conditions at the nozzle exit are obtained by using an explicit, fourth-order Runge–Kutta method. Various geometrical shapes are obtained depending on the mass flow rate, angular momentum, Weber number and the boundary conditions imposed on sheet thickness, radial sheet-centerline location, as well as their derivatives, at the nozzle exit. For the considered diverging 'conical' sheets, the steady-state solutions are recovered by numerical solution of the transient problem and by careful consideration of the necessary boundary conditions, the latter employing information on the propagation characteristics of wave groups or energy on these sheets.

Film blowing (i.e. the radial expansion of an infinite annular sheet) from excess swirl has also been analyzed identifying an absolutely stable equilibrium point.

The nonlinear breakup of initially steady 'conical' sheets due to modulations of the axial and/or transverse sheet velocity at the orifice has been studied numerically. For the cases analyzed, sheet thinning due to sheet divergence does not fundamentally change the characteristics of the nonlinear sheet breakup observed for swirling but nondiverging annular sheets. Nonlinear effects lead to the formation of fluid rings with thinner shells connecting them. However, sheet thinning due to sheet divergence affects sheet-breakup lengths and breakup times. Comparison between annular sheets with swirl in a surrounding void and annular sheets with no swirl but nonzero gas-core pressure shows that swirl can significantly reduce nonlinear sheet-breakup lengths and breakup times. The comparison also suggests that: (1) the formation of bubbles between fluid rings observed for 'pressure-stabilized' annular sheets can be attributed to the assumption of a constant gas-core pressure in this case and (2) even without the aid of aerodynamic effects, swirling annular sheets will break faster than nonswirling ones. Three-dimensional simulations have shown that the axisymmetric mode of sheet distortion can dominate over existing low and moderate amplitude three-dimensional modes.

Acknowledgements

This research has been supported by the US Army Research Office through Grant/ Contract No. DAAH 04-96-1-0055 with Dr. David Mann as the program manager.

References

Bachalo, W.D., 2000. Spray diagnostics for the twenty-first century. Atom. Sprays 10 (3–5), 439–474.

Ballester, J.M., Dopazo, C., 1996. Drop size measurements in heavy oil sprays from pressure-swirl nozzles. Atom. Sprays 6 (4), 377–408.

Chung, I.P., Presser, C., Dressler, J.L., 1998. Effect of piezoelectric transducer modulation on liquid sheet disintegration. Atom. Sprays 8 (5), 479–502.

Cousin, J., Vich, G., Nally, J.F., 2000. Formation and primary breakup of conical liquid sheets discharged by pressure swirl injectors. Experimental and theoretical investigation. In: Proceedings of the 8th International Conference on Liquid Atom. Spray Sys. ICLASS, available on CD-rom.

Entov, V.M., Kestenboim, K.S., Rozhkov, A.N., Sharchevich, L.I., 1980. Dynamic equilibrium shape of a film of viscous or viscoelastic liquid. Izvestiya Akademii Nauk SSSR, Mekhanika Zhidkosti i Gaza 15(2), 9–18.

Finnicum, D.S., Weinstein, S.J., Ruschak, K.J., 1993. The effect of applied pressure on the shape of a two-dimensional liquid curtain falling under the influence of gravity. J. Fluid Mech. 255, 647–665.

Fraser, R.P., 1956. Liquid fuel atomization. In: Sixth International Symposium on Combustion Yale University, New Haven, pp. 687–701.

Hashimoto, H., Suzuki, T., 1991. Experimental and theoretical study of fine interfacial waves on thin liquid sheet. JSME Int. J., Ser. II 34 (3), 277–283.

Kawano, S., Hashimoto, H., Togari, H., Ihara, A., Suzuki, T., Harada, T., 1997. Deformation and breakup of an annular liquid sheet in a gas stream. Atom. Sprays 7, 359–374.

Kim, I., Sirignano, W.A., 2000. Three-dimensional wave distortion and disintegration of thin planar liquid sheets. J. Fluid Mech. 410, 147–183.

Lee, C.P., Wang, T.G., 1986. A theoretical model for the annular jet instability. Phys. Fluids 29, 2076–2085.

Lee, C.P., Wang, T.G., 1989. The theoretical model for the annular jet instability – revisited. Phys. Fluids A 1, 967–974.
Lefebvre, A.H., 1989. Atomization and Sprays. Hemisphere, New York.
Mehring, C., Sirignano, W.A., 1999. Nonlinear capillary wave distortion and disintegration of thin planar liquid sheets. J. Fluid Mech. 388, 69–113.
Mehring, C., Sirignano, W.A., 2000a. Axisymmetric capillary waves on thin annular liquid sheets Part I: temporal stability. Phys. Fluids 12 (6), 1417–1439.
Mehring, C., Sirignano, W.A., 2000b. Axisymmetric capillary waves on thin annular liquid sheets. Part II: spatial development. Phys. Fluids 12 (6), 1440–1460.
Panchagnula, M.V., Santangelo, P.J., Sojka, P.E., 1995. On the three-dimensional instability of a swirling, annular, inviscid liquid sheet subject to unequal gas velocities. In: Proceedings of the 8th Annual Conference on Liquid Atom. Spray Sys., ILASS, North and South America, pp. 54–58.
Panchagnula, M.V., Sojka, P.E., Bajaj, A.K., 1998. The nonlinear breakup of annular liquid sheets. In: Proceedings of the 11th Annual Conference on Liquid Atom. Spray Sys., ILASS, North and South America, pp. 170–174.
Panchagnula, M.V., Sojka, P.E., Santangelo, P.J., 1996. On the three-dimensional instability of a swirling, annular, inviscid liquid sheet subject to unequal gas velocities. Phys. Fluids 8, 3300–3312.
Ramos, J.I., 1992. Annular liquid jets: formulation and steady-state analysis. Z. Angew. Math. Mech. 72, 565–589.
Ramos, J.I., 1994. The fluid dynamics of thin annular liquid jets. Current Topics Phys. Fluids 1, 75–112.
Ramos, J.I., 1995a. Fluid dynamics of slender, thin, annular liquid jets. Int. J. Numer. Meth. 21, 735–761.
Ramos, J.I., 1995b. On the growth of underpressurized annular liquid jets. Appl. Math. Model. 19, 13–25.
Ramos, J.I., 1995c. Hopf bifurcation in annular liquid jets with mass transfer. Int. J. Numer. Meth. Fluids 20, 1293–1314.
Ramos, J.I., 1995d. The effects of fluctuating body forces on annular liquid jets. Arch. Appl. Mech. 65, 548–563.
Ramos, J.I., 1996a. Irrotational, annular liquid jets. J. Math. Anal. Appl. 202, 538–554.
Ramos, J.I., 1996b. Force fields on inviscid, slender, annular liquid jets. Int. J. Numer. Meth. Fluids 23, 221–239.
Ramos, J.I., 1996c. G-jitter effects on mass transfer in annular liquid jets. Int. J. Numer. Meth. Heat Fluid Flow 6, 17–28.
Ramos, J.I., 1996d. One-dimensional models of steady, inviscid, annular liquid jets. Appl. Math. Model. 20, 593–607.
Ramos, J.I., 1997a. Mass transfer in annular liquid jets in the presence of liquid flow rate fluctuations. Appl. Math. Model. 21, 363–369.
Ramos, J.I., 1997b. Analysis of annular liquid membranes and their singularities. Meccanica 32, 279–293.
Ramos, J.I., 1998. Annular liquid jets and other axisymmetric free-surface flows at high Reynolds numbers. Appl. Math. Model. 22, 423–452.
Ramos, J.I., 1999. An adaptive method for heat transfer in annular liquid jets. Int. J. CFD 11, 285–302.
Richtmyer, R.D., Morton, K.W., 1967. Difference Methods for Initial-Value Problems, 2nd ed. Wiley, New York.
Schmidt, U.T., Sojka, P.E., 1999. Air-assist pressure-swirl atomization. Atom. Sprays 9, 173–192.
Squire, H.B., 1953. Investigation of the instability of a moving liquid film. Br. J. Appl. Phys. 4, 167–169.
Tadmor, Z., Gogos, C.G., 1979. Principles of Polymer Processing. Wiley, New York.
Taylor, G.I., 1959a. The dynamics of thin sheets of fluid, I. Water bells. Proc. R. Soc. London, Ser. A 253, 289–295.
Taylor, G.I., 1959b. The dynamics of thin sheets of fluid, III. Disintegration of fluid sheets. Proc. R. Soc. London, Ser. A 253, 313–321.
Yarin, A.L., 1993. Free Liquid Jets and Films: Hydrodynamics and Rheology. Longman, New York.
York, J.L., Stubbs, H.E., Tek, M.R., 1953. The mechanism of disintegration of liquid sheets. Trans. ASME 75 1279–1286.